



# CHORUS

This is the accepted manuscript made available via CHORUS. The article has been published as:

## Tunable many-body interactions in semiconducting graphene: Giant excitonic effect and strong optical absorption

Marc Dvorak and Zhigang Wu

Phys. Rev. B **92**, 035422 — Published 21 July 2015

DOI: [10.1103/PhysRevB.92.035422](https://doi.org/10.1103/PhysRevB.92.035422)

# Tunable Many-Body Interactions in Semiconducting Graphene: Giant Excitonic Effect and Strong Optical Absorption

Marc Dvorak and Zhigang Wu\*

*Department of Physics, Colorado School of Mines, Golden, CO 80401, USA*

(Dated: July 1, 2015)

Electronic and optical properties of graphene depend strongly on many-body interactions. Employing the highly accurate many-body perturbation approach based on Green's functions, we find a large renormalization over independent particle methods of the fundamental band gaps of semiconducting graphene structures with periodic defects. Additionally, their exciton binding energies are larger than 0.4 eV, suggesting significantly strengthened electron-electron and electron-hole interactions. Their absorption spectra show two strong peaks whose positions are sensitive to the defect fraction and distribution. The strong near-edge optical absorption and excellent tunability make these two-dimensional materials promising for optoelectronic applications.

## I. INTRODUCTION

Since the discovery of graphene<sup>1-4</sup>, the physics of two-dimensional (2D) materials, including boron nitride (BN) monolayer<sup>5</sup> and transition-metal dichalcogenides<sup>6</sup>, has been a rapidly evolving research field<sup>7</sup>. Graphene possesses exceptional charge carrier mobilities<sup>8</sup>, unusual optical properties<sup>9,10</sup>, and exotic topological phases<sup>11,12</sup>, showing great promise in replacing bulk semiconductors to build next-generation optoelectronic devices<sup>13,14</sup>. In order to realize this vision, however, electronic and optical properties of graphene must be tunable. One practical approach is patterning graphene periodically with vacancies<sup>13</sup>, passivants<sup>15</sup>, dopants<sup>16</sup> etc. Certain patterns of defects on graphene induce long-range order that causes a nonzero scattering matrix element between Dirac points and opens a sizable band gap ( $E_g$ ). The magnitude of  $E_g$  in these semiconducting materials depends on defect size, type, and distribution<sup>17-23</sup>.

In contrast to electronic band structure, which can be well described within the a single-quasiparticle (QP) picture, excitonic effects and optical spectra depend sensitively on two-QP (electron-hole) interactions as well, especially for low-dimensional materials. In low dimensional materials, low electronic screening and the close proximity of electron and hole lead to strengthened electron-electron and electron-hole interactions. Furthermore, the electron-electron interactions between the single-QP excitations can't be accurately determined by single-particle methods, such as density functional theory (DFT), which tends to severely underestimate  $E_g$ .<sup>24-26</sup> The *GW* approximation<sup>24-26</sup> is the state-of-the-art approach to compute single-QP energies, and solving the Bethe-Salpeter equation (BSE)<sup>26-28</sup> for correlated electron-hole excitations has been remarkably successful in quantifying excitonic effects in low-dimensional materials<sup>9,29,30</sup>. But *GW*-BSE calculations have not been performed for these semiconducting graphene structures because of their large cell sizes.

In this article, the QP energies and optical spectra of semiconducting graphene structures are computed to reveal the effects of defect size, geometric arrangement,

and type on many-body interactions involved in electronic excitations. We consider vacancy defects that form graphene nanomeshes (GNMs) in hexagonal and rectangular arrangements, and BN doped graphene in a hexagonal arrangement. Our results show that DFT underestimates  $E_g$  of these materials by about 50%, suggesting strong many-body interactions. The independent-QP absorption spectra miss essential features of the optical spectra that are attributed solely to the electron-hole interaction. Each BSE absorption spectrum shows two strong and isolated peaks below a continuum of exciton states. Excitons are strongly bound, with giant binding energies ( $E_b$ ) ranging from 0.46 – 0.81 eV, in comparison to  $E_g$  of 1.3 – 2.2 eV. The excitons form a non-hydrogenic series and individual exciton wave functions show a  $\Gamma$ -centered ring structure in the Brillouin zone. The absorption edge is also strongly dependent on defect size. By varying the fraction of the unit cell occupied by the defect, it is possible to tune the optical gap to essentially any value below  $\sim 1.4$  eV, making these materials promising for optoelectronic applications.

## II. MODELLING

We use four parameters ( $n_1, m_1, n_2, m_2$ ) to denote the translation vectors ( $\mathbf{R}_1$  and  $\mathbf{R}_2$ ) of a defected graphene supercell:  $\mathbf{R}_1 = n_1 \mathbf{a}_1 + m_1 \mathbf{a}_2$  and  $\mathbf{R}_2 = n_2 \mathbf{a}_1 + m_2 \mathbf{a}_2$ <sup>17,18</sup>, with  $\mathbf{a}_1$  and  $\mathbf{a}_2$  the primitive translation vectors of pristine graphene. As long as the defect has average hexagonal symmetry<sup>31</sup>, the  $\mathbf{K} \leftrightarrow \mathbf{K}'$  scattering condition that opens a band gap is equivalent to  $n_1 - m_1 = 3p$  and  $n_2 - m_2 = 3q$  for integers  $p$  and  $q$ . In this work, we consider  $(n_1, m_1, n_2, m_2) = (6, 0, 0, 6)$  and  $(6, -6, 3, 3)$  supercells. The  $(6, 0, 0, 6)$  hexagonal supercell has both edges along the zigzag direction, while the  $(6, -6, 3, 3)$  rectangular supercell has one edge along an armchair direction and the other along a zigzag direction. Here we refer to these two systems simply as hexagonal and rectangular, and consider vacancy and BN doping defects that occupy 6 C (one hexagonal ring) and 12 C atoms. The four systems investigated are shown on the left side of Fig. 1.

### III. COMPUTATIONAL METHODS

Our *ab-initio* *GW* calculations are performed on a  $4 \times 4$   $\mathbf{k}$ -point grid (equivalent to a  $24 \times 24$   $\mathbf{k}$ -point sampling in the Brillouin zone of pristine graphene for the  $(6, 0, 0, 6)$  structure) using the QUANTUM ESPRESSO<sup>32</sup> and BerkeleyGW<sup>33</sup> packages. DFT calculations are performed with the PBE-GGA<sup>34</sup>, norm-conserving pseudopotentials, and a cutoff energy of 60 Ry. We find the *GW* self-energies ( $\Sigma$ ) converged for the dielectric function with a cutoff energy of 10 Ry. Unlike the 2D transition-metal dichalcogenides<sup>29,35</sup>, these systems do not show localized states, leading to fast convergence of  $\Sigma$ . Summations over empty states to compute  $\Sigma$  include  $5 \times 10^3$  unoccupied bands, so that QP energies are converged to within 0.1 eV. We use the generalized plasmon-pole model of Hybertsen and Louie<sup>24</sup>.

### IV. RESULTS AND DISCUSSION

#### A. Electronic Band Structures

The right four panels of Fig. 1 show the electronic band structures of the four systems studied, which are all semiconducting with a direct gap at  $\Gamma$ . We note that due to band folding, the Dirac points of pristine graphene are located at the  $\Gamma$ -point of the Brillouin zone of these supercells. The intervalley scattering induced by periodic defects removes the Dirac points and opens a band gap at the  $\Gamma$ -point. All of them have two isolated (or nearly isolated) valence (conduction) bands near the Fermi energy below (above) the gap. The *GW* band gap is almost double the DFT gap, with the renormalization factor  $E_g^{GW}/E_g^{DFT} \approx 1.8 - 2.1$ , because of low screening and strong electron-electron interactions in 2D materials compared with their 3D counterparts.

In GNMs, as the hole size increases,  $E_g$  increases, scaling roughly  $\propto \sqrt{N_C^{\text{removed}}/N_C^{\text{original}}}$ , based on the tight-binding model proposed by Pedersen *et al.*<sup>36</sup>, with  $N_C^{\text{removed}}$  and  $N_C^{\text{original}}$  the numbers of removed and original C atoms, respectively. Other similar scaling rules for structurally modified graphene based on tight-binding or DFT have also been proposed<sup>17-19,37</sup>. We expect  $E_g$  obtained from our *GW* calculations to also obey the same scaling law (with quantitatively more accurate parameters). In principle, one can tune  $E_g$  in patterned graphene to any desired value by varying defect percentage or supercell size. However, for the same defect percentage,  $E_g$  can also vary considerably, e.g.,  $E_g = 1.27$  eV in the rectangular GNM shown in Fig. 1c, compared to  $E_g = 1.58$  eV in the hexagonal GNM (Fig. 1a) with the same  $N_C^{\text{removed}}$  and  $N_C^{\text{original}}$ . We note that this effect is in contrast to simple scaling rules based solely on  $N^{\text{removed}}$ . Clearly, the geometric arrangement of the defects has a nontrivial effect on the band gap as well. Finally, Fig. 1b and 1d provide a comparison of vacancy

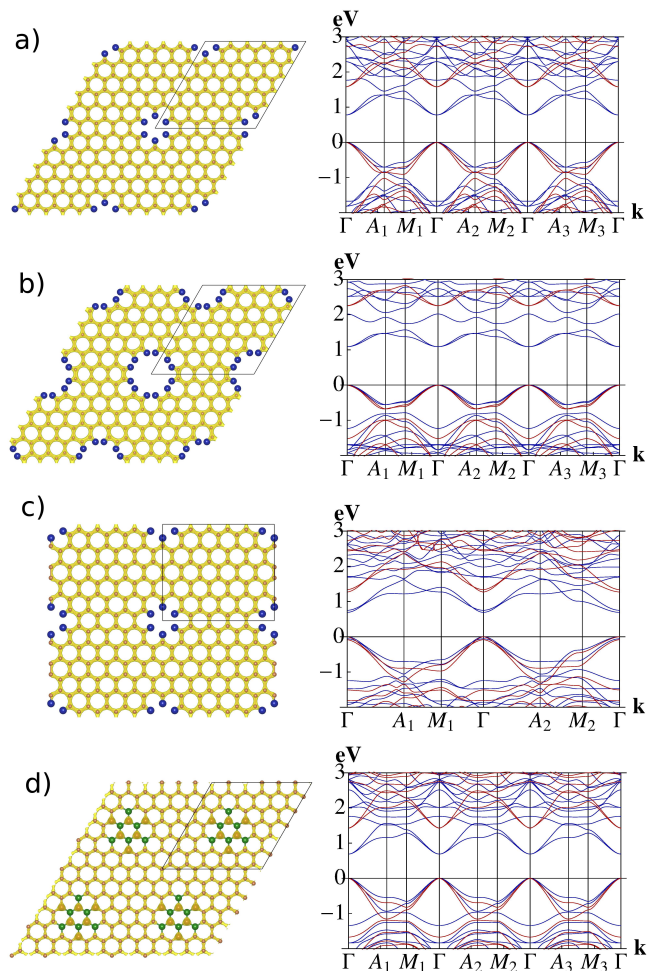


FIG. 1. (color online) Crystal (left column) and electronic band (right column) structures of defected graphene structures. Yellow isosurfaces (left) indicate the total charge density. Blue and red lines (right) correspond to DFT and *GW* band structures, respectively. Hole edges are passivated by hydrogen (blue dots). (a)  $(6, 0, 0, 6)$  GNM with a 6-C hole. (b)  $(6, 0, 0, 6)$  GNM with a 12-C hole. (c)  $(6, -6, 3, 3)$  GNM with a 6-C hole. (d)  $(6, 0, 0, 6)$  BN doped graphene with 12 C atoms replaced by hexagonal BN (green and gold dots). Band gaps, in eV, are (a) (DFT, *GW*) = (0.78, 1.58), (b) (1.09, 2.26), (c) (0.69, 1.27), and (d) (0.69, 1.43).

defects versus BN dopants. For the same defect size, BN dopants are a smaller perturbation than vacancies and open a considerably smaller band gap (reduced by about one third). The electronic structure shown in Fig. 1d is similar to that of the corresponding GNM (Fig. 1b) in spite of the fact that the GNM preserves the AB sublattice symmetry and BN dopants do not. The combined effects of sublattice imbalance and intervalley scattering are explored in our previous work<sup>18</sup>.

## B. Optical Properties

Our primary focus in this work is the optical properties of defected graphene. To account for the electron-hole interaction, we use BerkeleyGW to solve the BSE for the two-QP eigenstates<sup>33</sup>. We compute the electron-hole interaction on the same  $4 \times 4$  grid of  $\mathbf{k}$ -points, and then interpolate the matrix elements onto a  $20 \times 20$   $\mathbf{k}$ -point grid. For the hexagonal systems, this is equivalent to a  $120 \times 120$   $\mathbf{k}$ -point sampling of a graphene primitive cell. Such a dense  $\mathbf{k}$ -point sampling is required to converge exciton eigenvalues within 40 meV. DFT wave functions are used as the basis, with  $GW$  QP energies used in place of DFT eigenvalues. The screened interaction is evaluated up to 10 Ry, and all independent-QP transitions up to 6 eV are used to construct the Hamiltonian.

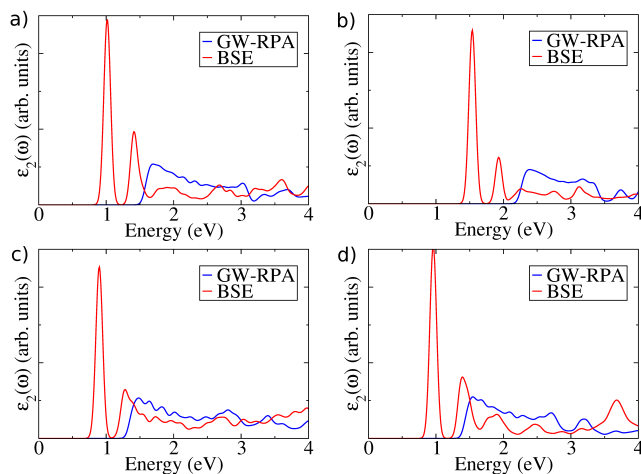


FIG. 2. (color online) Imaginary part of the dielectric function for hexagonal systems with a (a) 6-C hole, (b) 12-C hole, (c) rectangular system with a 6-C hole, and (d) hexagonal system with 12 C atoms replaced by BN dopants.

Fig. 2 shows the imaginary dielectric functions ( $\epsilon_2$ ) for the same four systems as shown in Fig. 1. In each case, the excitonic absorption edge is red-shifted by roughly 0.5 eV compared to the  $GW$ -RPA (random phase approximation) spectrum. The BSE spectra all show two prominent absorption peaks before reaching a continuum of exciton states, which are missing from the non-interacting single-QP estimation. The oscillator strengths of these peaks are enhanced considerably compared to any of the peaks in the non-interacting spectra.

Specifically, there are two absorption peaks at 1.02 and 1.41 eV in Fig. 2a; below 1.02 eV, there exists a single dark state at 0.97 eV. Here optically dark states have an oscillator strengths more than four orders weaker than those of states contributing to the main absorption peaks, and in general they are symmetry-forbidden combinations of bands near the  $\Gamma$ -point. This dark state is bound by  $E_b = 0.61$  eV below the band gap. Such strongly bound excitons are typical of low-dimensional systems,

and comparable values have been theoretically predicted and observed experimentally in 2D materials<sup>29,30,35,38</sup>. In comparison, the electron-hole binding energy in covalently bonded bulk semiconductors is typically only tens of meV, although certain ionic compounds have Frenkel excitons bound by hundreds of meV<sup>39,40</sup>. It is important to note that our calculations are performed for a free-standing GNM without substrate. Experimentally, GNMs are likely to be fabricated on a substrate, which could reduce  $E_b$  and shift absorption peaks because of the enhanced screening<sup>35</sup>.

In the following, we analyze excitons of the GNM shown in Fig. 1a. The first absorption peak is comprised of three degenerate states (excitons 2 – 4) originating from transitions directly at  $\Gamma$ , which corresponds to  $\mathbf{K}$  and  $\mathbf{K}'$  in pristine graphene. The optical absorption edge in transition metal dichalcogenides<sup>29,35</sup> also occurs at  $\mathbf{K}$  and  $\mathbf{K}'$  points in the Brillouin zone. Fig. 3a shows the modulus squared of the third exciton wave function and the weights in the Brillouin zone of electron-hole pairs contributing to the exciton. Away from  $\Gamma$ , the contributions to the exciton decrease rapidly. The first four excitons, including the dark state, all have similar character: they are approximately azimuthally symmetric in real space and localized functions with a single peak in  $\mathbf{k}$ -space. These four states are made of different mixings of the two degenerate valence and two degenerate conduction bands at  $\Gamma$ ; thus the low energy absorption is dominated by these nearly isolated pairs of valence and conduction bands near the band gap in Fig. 1a.

Next, there are two degenerate dark states with similar character at 1.32 eV. Shown in Fig. 3b, these states are primarily comprised of six transitions in a ring surrounding  $\Gamma$ . The six-fold symmetric maxima in  $\mathbf{k}$ -space are located along the  $\Gamma - M$  directions of the Brillouin zone. In real space, the wave function has two lobes, resembling a  $p$ -type wave function. In general, we find that exciton spectra of defected graphene do not resemble a hydrogenic series, agreeing with previous work on 2D materials<sup>29,30,41</sup>. Certain exciton wave functions, however, still show a strong  $s$ - or  $p$ -type character. Excitons 7–10 are two closely spaced pairs of degenerate states. In real space (Fig. 3c), the exciton has a preferred direction but no obvious structure; in reciprocal space, however, the  $\mathbf{k}$ -point weights form two lobes centered on a line going through  $\Gamma$ . For these four states, the orientation of the lobes varies between the  $\Gamma - M$  and  $\Gamma - A$  directions of the Brillouin zone with a minimum weight at  $\Gamma$ .

The next optically active state is the 14th exciton eigenstate, contributing to the second absorption peak at 1.41 eV. In  $\mathbf{k}$ -space, the weights are peaked sharply at  $\Gamma$  – sharper than Fig. 3a – pass through a minimum, and then form a nearly continuous ring around  $\Gamma$ . This state, together with higher exciton states, bear resemblance to the states shown in Fig. 3 but acquire additional nodes in  $\mathbf{k}$ -space as the excitation energy increases. Not until the continuum of states are there significant contributions to the optical absorption beyond the pairs of valence and

conduction bands near the band gap (see Fig. 1). In the continuum, the exciton states have a structure near the  $\Gamma$ -point similar to those shown in Fig. 3 but slowly gain weight at  $k$ -points further away from  $\Gamma$ .

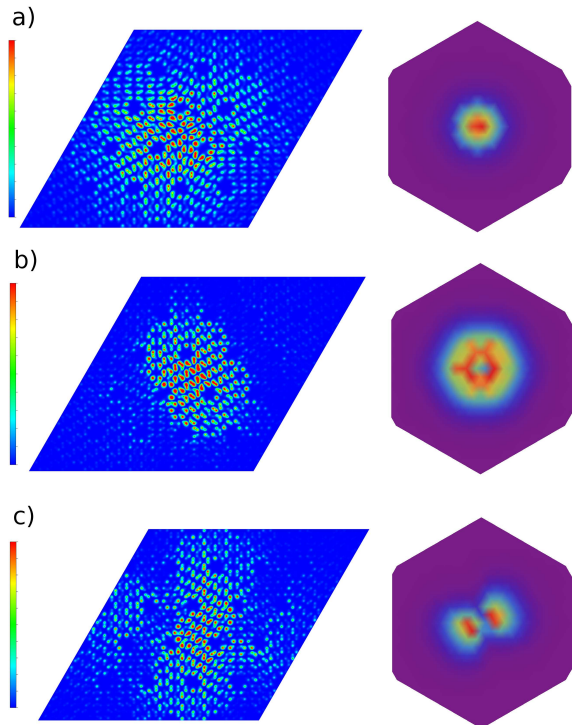


FIG. 3. (color online) Real space plots of the exciton wave function modulus squared (left column) and weights in the Brillouin zone (right column) for the (a) third, (b) fifth, and (c) seventh lowest exciton eigenstates in a hexagonal GNM shown in Fig. 1a. The hole in an exciton wave function is fixed at the center of the supercell, and the modulus squared of the electron coordinate is shown in the density plots. Real space plots are in a  $6 \times 6$  supercell (left), and the purple hexagon is the Brillouin zone (right).

Fig. 2b shows  $\epsilon_2$  for a hexagonal system with a 12-C hole. Due to its larger band gap, the absorption edge for this system is substantially blue-shifted compared to that in Fig. 2a. Otherwise, both hexagonal GNMs share the same basic features, as expected. Here, the lowest exciton is bound by  $E_b = 0.81$  eV, which is  $\approx 1/3$  stronger than that in the hexagonal supercell with a 6-C hole. Furthermore, our calculations show that electronic screening is reduced as the electron density decreases with increasing hole size, enhancing the electron-hole interaction. In GNMs, regions of weak screening exist not only outside of the graphene plane, as in all 2D materials, but also *in plane* in the vacuum regions of holes. As hole size increases in GNMs, the anti-screening effect seen in 2D materials<sup>41</sup> may be enhanced from in plane contributions. Additionally, a larger hole forces greater confinement of the electron and hole between defects. This increased physical overlap of their wave functions also serves to

enhance  $E_b$ . Finally, we observe flatter bands and an increased effective mass for electrons and holes as defect size increases (Fig. 1). In the hydrogenic model for excitons,  $E_b$  increases with increasing exciton effective mass, in agreement with our BSE results.

We also consider the effect of geometric configuration of defects on  $\epsilon_2$ . Fig. 2c plots  $\epsilon_2$  for the rectangular GNM (Fig. 1c). The rectangular system shows a slight red shift of its absorption spectrum compared with its corresponding hexagonal GNM, but its absorption generally has the same character as that of the hexagonal system. This is not surprising, given the similarities of the near gap bands plotted in Fig. 1. However, because of the reduced symmetry of the rectangular system, several states that were completely dark in the hexagonal geometry now appear as very small shoulders near the main absorption peaks, though their enhancement is not significant enough to dramatically alter the shape of  $\epsilon_2$ . Interestingly, the lowest exciton in the rectangular system is bound by only 0.46 eV, noticeably less than  $E_b$  in the corresponding hexagonal system with the same number of C atoms and hole size. One possible explanation for this difference is less confinement of electron and hole in a rectangular supercell compared to a hexagonal cell. If we consider the largest circle that can fit on each supercell between the boundaries of defects, it is straightforward to show that the circle in the rectangular supercell has a larger radius than the circle in the hexagonal supercell. If we consider this ‘confinement circle’ as a crude measure of electron-hole confinement, the trend predicted by the circle radius agrees with the trend in our calculated values of  $E_b$ .

Finally, we compute the optical properties of the BN doped system shown in Fig. 1d. Fig. 2b and d provide a comparison of  $\epsilon_2$  for a GNM with a 12-C hole and a graphene sheet with 12 C atoms replaced by BN. There is a large red-shift of  $> 0.5$  eV of the BN spectra because of its much reduced band gap, but the overall features of the absorption remain the same. The most striking difference between these two materials is their difference in exciton binding energy:  $E_b^{\text{GNM}} = 0.81$  eV while  $E_b^{\text{BN-doped}} = 0.48$  eV. As with the comparison of  $E_b$  between GNMs with 12-C and 6-C holes, increased electronic screening is likely responsible for the large reduction in  $E_b$  seen in BN-doped systems. Rather than removing electrons by increasing hole size in a GNM, the average electron density in BN doped graphene actually increases compared to its corresponding GNM. Our results demonstrate great tunability of the optical band gap and exciton binding energy in periodically defected graphene.

## V. SUMMARY

In conclusion, we have reported *ab-initio* results for the electronic band structure and optical properties of 2D graphene-based semiconductors obtained from *GW*-BSE

computations. The QP band gaps of these materials are roughly twice their DFT values, while the optical absorption shows two prominent peaks below the continuum of exciton states. Low-energy excitons are strongly bound and composed of transitions mixing the two highest valence bands with the two lowest conduction bands near the  $\Gamma$ -point. Our results demonstrate great sensitivity of structurally modified graphene's electronic and optical properties to size, type, and distribution of the defects, thus these 2D materials can be customized to make better optoelectronic devices. For example, varying the hole size in a GNM could tune the absorption edge to any value in the 0 – 1.4 eV range; due to its extremely efficient optical absorption, a layered GNM structure with varying hole and supercell size could be an ideal absorber material for photovoltaics. Furthermore, strong Coulomb

interactions and a relatively small band gap would suggest efficient multi-exciton generation<sup>42</sup>, while the strong and isolated absorption peaks make these materials good candidates for light-emitting diodes.

## ACKNOWLEDGMENTS

This work was supported by U.S. DOE Early Career Award (Grant No. DE-SC0006433). Computations were carried out at the Golden Energy Computing Organization at CSM and the National Energy Research Scientific Computing Center (NERSC). The authors thank M. Lusk and D. Wood for insightful discussions.

- 
- \* zhiwu@mines.edu
- <sup>1</sup> K. S. Novoselov, A. K. Geim, S. V. Morozov, D. Jiang, Y. Zhang, S. V. Dubonos, I. V. Grigorieva, and A. A. Firsov, *Science* **306**, 666 (2004).
  - <sup>2</sup> K. S. Novoselov, A. K. Geim, S. V. Morozov, D. Jiang, M. I. Katsnelson, I. V. Grigorieva, S. V. Dubonos, and A. A. Firsov, *Nature* **438**, 197 (2005).
  - <sup>3</sup> A. K. Geim and K. S. Novoselov, *Nature Mater.* **6**, 183 (2007).
  - <sup>4</sup> A. Castro Neto, F. Guinea, N. Peres, K. Novoselov, and A. Geim, *Rev. Mod. Phys.* **81**, 109 (2009).
  - <sup>5</sup> A. Nagashima, N. Tejima, Y. Gamou, T. Kawai, and C. Oshima, *Phys. Rev. Lett.* **75**, 3918 (1995).
  - <sup>6</sup> K. Mak, C. Lee, J. Hone, J. Shan, and T. Heinz, *Phys. Rev. Lett.* **105**, 136805 (2010).
  - <sup>7</sup> K. S. Novoselov, D. Jiang, F. Schedin, T. J. Booth, V. V. Khotkevich, S. V. Morozov, and A. K. Geim, *Proc. Nat. Acad. Sci.* **102**, 10451 (2005).
  - <sup>8</sup> A. S. Mayorov, R. V. Gorbachev, S. V. Morozov, L. Britnell, R. Jalil, L. A. Ponomarenko, P. Blake, K. S. Novoselov, K. Watanabe, T. Taniguchi, and A. K. Geim, *Nano Lett.* **11**, 2396 (2011).
  - <sup>9</sup> L. Yang, J. Deslippe, C.-H. Park, M. L. Cohen, and S. G. Louie, *Phys. Rev. Lett.* **103**, 186802 (2009).
  - <sup>10</sup> T. G. Pedersen, C. Flindt, J. Pedersen, A.-P. Jauho, N. A. Mortensen, and K. Pedersen, *Phys. Rev. B* **77**, 245431 (2008).
  - <sup>11</sup> D. Hsieh, Y. Xia, D. Qian, L. Wray, J. H. Dil, F. Meier, J. Osterwalder, L. Patthey, J. G. Checkelsky, N. P. Ong, A. V. Fedorov, H. Lin, A. Bansil, D. Grauer, Y. S. Hor, R. J. Cava, and M. Z. Hasan, *Nature* **460**, 1101 (2009).
  - <sup>12</sup> M. Z. Hasan and C. L. Kane, *Rev. Mod. Phys.* **82**, 3045 (2010).
  - <sup>13</sup> J. Bai, X. Zhong, S. Jiang, Y. Huang, and X. Duan, *Nature Nanotech.* **5**, 190 (2010).
  - <sup>14</sup> F. Schwierz, *Nature Nanotech.* **5**, 487 (2010).
  - <sup>15</sup> L. Ci, L. Song, C. Jin, D. Jariwala, D. Wu, Y. Li, A. Srivastava, Z. F. Wang, K. Storr, L. Balicas, F. Liu, and P. M. Ajayan, *Nature Mater.* **9**, 430 (2010).
  - <sup>16</sup> R. Balog, B. Jorgensen, L. Nilsson, M. Andersen, E. Rienks, M. Bianchi, M. Fanetti, E. Laegsgaard, A. Baraldi, S. Lizzit, Z. Sljivancanin, F. Besenbacher, B. Hammer, T. G. Pedersen, P. Hofmann, and L. Hornekaer, *Nature Mater.* **9**, 315 (2010).
  - <sup>17</sup> M. Dvorak, W. Oswald, and Z. Wu, *Sci. Rep.* **3**, 2289 (2013).
  - <sup>18</sup> M. Dvorak and Z. Wu, *Phys. Rev. B* **90**, 115415 (2014).
  - <sup>19</sup> W. Oswald and Z. Wu, *Phys. Rev. B* **85**, 115431 (2012).
  - <sup>20</sup> R. Martinazzo, S. Casolo, and G. F. Tantardini, *Phys. Rev. B* **81**, 245420 (2010).
  - <sup>21</sup> B. Xu, Y. H. Lu, Y. P. Feng, and J. Y. Lin, *J. Appl. Phys.* **108**, 073711 (2010).
  - <sup>22</sup> F. Ouyang, S. Peng, Z. Liu, and Z. Liu, *ACS Nano* **5**, 4023 (2011).
  - <sup>23</sup> R. Grassi, T. Low, and M. Lundstrom, *Nano Lett.* **11**, 4574 (2011).
  - <sup>24</sup> M. S. Hybertsen and S. G. Louie, *Phys. Rev. B* **34**, 5390 (1986).
  - <sup>25</sup> W. G. Aulbur, L. Jnsson, and J. W. Wilkins (Academic Press, 1999) pp. 1 – 218.
  - <sup>26</sup> G. Onida, L. Reining, and A. Rubio, *Rev. Mod. Phys.* **74**, 601 (2002).
  - <sup>27</sup> A. L. Fetter and J. D. Walecka, *Quantum theory of many-particle systems* (McGraw-Hill, 1971).
  - <sup>28</sup> M. Rohlfing and S. G. Louie, *Phys. Rev. B* **62**, 4927 (2000).
  - <sup>29</sup> D. Y. Qiu, F. H. da Jornada, and S. G. Louie, *Phys. Rev. Lett.* **111**, 216805 (2013).
  - <sup>30</sup> K. He, N. Kumar, L. Zhao, Z. Wang, K. F. Mak, H. Zhao, and J. Shan, *Phys. Rev. Lett.* **113**, 026803 (2014).
  - <sup>31</sup> M. Dvorak and Z. Wu, *Nanoscale* **7**, 3645 (2015).
  - <sup>32</sup> P. Giannozzi, S. Baroni, N. Bonini, M. Calandra, R. Car, C. Cavazzoni, D. Ceresoli, G. L. Chiarotti, M. Cococcioni, I. Dabo, A. D. Corso, S. de Gironcoli, S. Fabris, G. Fratesi, R. Gebauer, U. Gerstmann, C. Gougoussis, A. Kokalj, M. Lazzeri, L. Martin-Samos, N. Marzari, F. Mauri, R. Mazzarello, S. Paolini, A. Pasquarello, L. Paulatto, C. Sbraccia, S. Scandolo, G. Sclauzero, A. P. Seitsonen, A. Smogunov, P. Umari, and R. M. Wentzcovitch, *J. Phys.: Condens. Matter* **21**, 395502 (2009).
  - <sup>33</sup> J. Deslippe, G. Samsonidze, D. A. Strubbe, M. Jain, M. L. Cohen, and S. G. Louie, *Comp. Phys. Commun.* **183**, 1269 (2012).
  - <sup>34</sup> J. P. Perdew, K. Burke, and M. Ernzerhof, *Phys. Rev. Lett.* **77**, 3865 (1996).

- <sup>35</sup> M. M. Ugeda, A. J. Bradley, S.-F. Shi, F. H. da Jornada, Y. Zhang, D. Y. Qiu, W. Ruan, S.-K. Mo, Z. Hussain, Z.-X. Shen, F. Wang, S. G. Louie, and M. F. Crommie, *Nature Mater.* **4061** (2014).
- <sup>36</sup> T. G. Pedersen, C. Flindt, J. Pedersen, N. A. Mortensen, A.-P. Jauho, and K. Pedersen, *Phys. Rev. Lett.* **100**, 136804 (2008).
- <sup>37</sup> R. Petersen and T. G. Pedersen, *Phys. Rev. B* **80**, 113404 (2009).
- <sup>38</sup> M. Bernardi, M. Palumbo, and J. C. Grossman, *Phys. Rev. Lett.* **108**, 226805 (2012).
- <sup>39</sup> M. Rohlfing and S. G. Louie, *Phys. Rev. Lett.* **81**, 2312 (1998).
- <sup>40</sup> M. Dvorak, S.-H. Wei, and Z. Wu, *Phys. Rev. Lett.* **110**, 016402 (2013).
- <sup>41</sup> A. Chernikov, T. C. Berkelbach, H. M. Hill, A. Rigosi, Y. Li, O. B. Aslan, D. R. Reichman, M. S. Hybertsen, and T. F. Heinz, *Phys. Rev. Lett.* **113**, 076802 (2014).
- <sup>42</sup> G. Nair, L.-Y. Chang, S. M. Geyer, and M. G. Bawendi, *Nano Lett.* **11**, 2145 (2011).